Available online at www.sciencedirect.com
SCIENCE DIRECT®
Journal of Electron Spectroscopy and Related Phenomena 149 (2005) 20–28
JOURNAL OF ELECTRON SPECTROSCOPY and Related Phenomena
www.elsevier.com/locate/elspec

Electron momentum spectroscopy of light and heavy targets

M. Vos*, C. Bowles, A.S. Kheifets, M.R. Went

Atomic and Molecular Physics Laboratories, Research School of Physical Sciences and Engineering, The Australian National University, Canberra 0200, Australia

Received 19 May 2005; received in revised form 6 June 2005; accepted 8 June 2005
Available online 8 August 2005

Abstract

Electron momentum spectroscopy (EMS) measures the spectral function of electrons in matter directly, provided that multiple scattering effects are negligibly small. Even for the thinnest films this is not the case and one has to correct for multiple scattering effects in order to retrieve the spectral function. Both elastic and inelastic scattering effects affect the measurement. Elastic scattering is expected to increase greatly with increasing atomic number, much more so than inelastic scattering. For this reason EMS was thought to be of limited value for heavy targets. Here, we present data for carbon, silicon and gold and show that they are affected in different ways by multiple scattering. The gold sample has poor count rate, but in the spectra the multiple scattering effects *appear* rather minor. Carbon and silicon on the other hand have good count rates, but the spectra are strongly affected by multiple scattering. Monte Carlo simulations are used to try to understand these effects. Rather surprisingly the EMS spectra for heavy elements are of comparable quality to those of lighter elements.

Keywords: Electron momentum spectroscopy; Elastic scattering; Inelastic scattering band structure

1. Introduction

Electron momentum spectroscopy (EMS) is a scattering experiment that is able to determine the electronic structure of matter [1]. In this experiment an incoming electron with several keV energy has a binary collision with an electron in the target. Because of the energy transfer in the collision the target electron is ejected and both scattered and ejected electrons are detected in coincidence (for this reason the technique is often referred to as (e,2e) spectroscopy). The difference of the sum of the (measured) energy of the outgoing electrons ($E_{1,2}$) and that of the incoming electron (E_0) is the ionisation energy ε:

$$\varepsilon = E_0 - E_1 - E_2 \tag{1}$$

In the same way the difference of the sum of the momenta of the outgoing electrons ($\mathbf{k}_1 + \mathbf{k}_2$) and the incoming momentum $\mathbf{k}_0$ is the recoil momentum $\mathbf{q}$ of the target:

$$\mathbf{q} = \mathbf{k}_0 - \mathbf{k}_1 - \mathbf{k}_2 \tag{2}$$

The frequency with which a coincidence event is observed with a certain ε, $\mathbf{q}$ combination is proportional to the magnitude of the spectral function $A(\varepsilon, \mathbf{q})$. In an independent particle approximation the measured intensity at ε, $\mathbf{q}$ is proportional to the probability that a target electron has binding energy ε and momentum $-\mathbf{q}$.

This technique works beautifully for gas-phase targets where the target density is low, and the (e,2e) event is virtually always the only scattering event [1,2]. For condensed matter the probability that additional scattering events occur before and/or after the (e,2e) event is significant, even for the thinnest film. If the incoming electron, or one of the outgoing electrons is deflected by a nucleus (elastic scattering) its momentum changes and the wrong recoil momentum of the (e,2e) event is inferred. By the same token if one of the incoming and or outgoing electrons excites the target electron system (inelastic scattering, e.g. plasmon creation) its energy changes and the wrong value for ε is obtained.

* Corresponding author. Tel.: +61 2 61254985; fax: +61 2 61252452.
E-mail address: maarten.vos@anu.edu.au (M. Vos).

0368-2048/$ – see front matter © 2005 Elsevier B.V. All rights reserved.
doi:10.1016/j.elspec.2005.06.002

As the probability of interaction of the incoming and outgoing electrons decreases with increasing energy one can minimise the probability of multiple scattering by increasing the energy of the incoming and outgoing electrons. Hence, our present spectrometer operates at relative high energies ($E_0 = 50$ keV, $E_{1,2} \approx 25$ keV) [3] and the multiple scattering effects are small, at least for the thinnest films and low Z targets. The main quasi-particle structure is well resolved and can be compared directly to band structure calculations, but the data contain more information than just the dispersion. Good agreement between the experimental data and theory is only obtained, if one corrects the experiment for multiple scattering and one uses calculations that go beyond the independent particle approximation [4–6].

In this paper we want to explore these multiple scattering effects, especially the possibility of EMS from heavy targets. We compare the case of a light element and a heavy element. Changing the atomic number Z changes elastic and inelastic scattering cross sections, but the quality of the observed spectra remains surprisingly very similar. Only the coincidence count rate decreases with increasing Z. We also explore the relationship between sample thickness, coincidence count rate and spectral shape. The spectral function obtained experimentally for a heavy target such as Au reveals the electronic structure clearly, in spite of its large cross section for elastic and inelastic scattering.

2. Elastic and inelastic scattering cross sections

There are two approaches used to describe the effects of elastic scattering of electrons in solids. One approach is based on the dynamical theory of diffraction. It stresses the coherent nature of waves scattering from different atoms. This theory, as applied to the case of EMS, is outlined by Allen et al. [7] and Matthews [8]. Actual use of the dynamical theory of diffraction to interpret EMS experiment has been limited to one study [9] and this work deals only with diffraction effects for the incoming beam. Applying this theory for the outgoing electrons is complicated as our slit detectors measure a range of outgoing electrons (with varying diffraction conditions) simultaneously. Also uncertainties in sample thickness and orientation (e.g. due to a slight wrinkling of the film of 100 Å thick over the 0.1 mm beam area) result in an uncertainty in the input parameters for the calculation. In this approach the momentum of the incoming and outgoing electrons can change only by a reciprocal lattice vector.

Diffraction effects (shifting of intensity by a reciprocal lattice vector) have been observed in EMS spectra (e.g. [10]) but from the smooth background intensity distribution observed in EMS measurements it is also clear that incoherent (or thermal diffuse) scattering is important as well. These latter processes can be simulated using a Monte Carlo approach and this approach was successfully applied to the interpretation of EMS spectra [11]. In this approach the elastic scattering cross sections used for atoms in solids are usually those obtained from calculations for isolated atoms. This is justified because elastic scattering occurs mainly when the electron is subjected to a strong electric field, i.e. close to the nucleus. Here, there is little difference between the potential of an isolated atom and of an atom in a solid. In Fig. 1, we plot the differential elastic cross section as calculated using the program PWADIR of Mayol and Salvat [12].

It is immediately clear that the elastic scattering cross section from carbon is about an order of magnitude smaller than that of Au. Moreover, the deflection for scattering from Au will generally be larger than that for scattering from carbon. In Table 1, the total cross section obtained from this calculation is given, as well as the transport cross section. The larger transport cross section reflects again the fact that scattering from Au generally involves larger angles than scattering from C. The elastic mean free path λ_{el} is inversely proportional to the total cross section and the density of scatterers in the target N: $\lambda_{el} = 1/(\sigma_e N)$.

In contrast to elastic scattering, inelastic scattering is a process in the solid, rather than near a nucleus. It depends, among

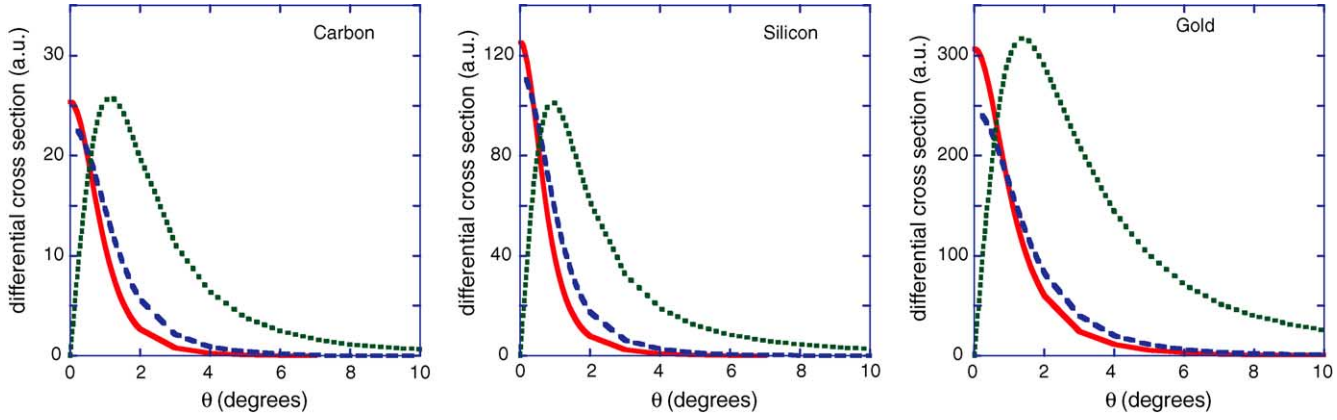

Fig. 1. The calculated differential elastic scattering cross section for 25 keV (dashed line) and 50 keV (solid line) electrons scattering from C (left), Si (central) and Au (right panel). Note the difference in the vertical scale of the three plots. The dotted line presents the (scaled) probability distribution that a 25 keV electron scatters over an angle θ integrated over all azimuthal angles.

Table 1
A summary of the relevant elastic cross section, transport cross section and elastic and inelastic mean free paths based on an approximate formula developed for XPS [13] and an approximate formula developed for EELS [14]

Element	E (keV)	σ_{el} (Å^{-2})	$\sigma_{tr.}$ (Å^{-2})	λ_{el} (Å)	λ_{in}^{XPS} (Å)	λ_{in}^{EELS} (Å)
Graphite	25	2.5×10^{-2}	1.3×10^{-4}	353	421	310
Graphite	50	1.3×10^{-2}	3.6×10^{-5}	680	775	630
Silicon	25	8.8×10^{-2}	6.0×10^{-4}	227	356	299
Silicon	50	4.8×10^{-2}	1.8×10^{-4}	416	654	510
Gold	25	4.6×10^{-1}	1.2×10^{-2}	37	170	188
Gold	50	3.1×10^{-1}	4.1×10^{-3}	55	310	322

other things, on the valence electron density in the solid. Unfortunately little information is available for the present energy range (25–50 keV). We calculated values using the semi-empirical expression given by Tanuma et al. [13] for electrons with energy E (in eV) and λ (in Å):

$$\lambda \approx E/[E_p^2 \beta \ln(\gamma E)] \quad (3)$$

with E_p the plasmon energy, β and γ tabulated parameters [13]. This formula was developed for XPS energies (up to 2 keV), and the current extrapolation to 50 keV is pushing the limits as, for example, relativistic corrections become significant at 50 keV.

An alternative approach is to use mean free path values obtained in the literature for electron energy loss spectroscopy (EELS) and extrapolate these to smaller energies. Here, a semi-empirical formula was proposed by Malis et al. [14] for λ in nm and E in keV.

$$\lambda \approx \frac{106FE}{E_m \ln(2\delta E/E_m)} \quad (4)$$

with $E_m = 7.4Z^{0.36}$, $\delta = \sqrt{E_p/E}$ and F a relativistic correction factor:

$$F = \frac{1 + (E/1022)}{(1 + (E/511))^2}$$

The similarity between Eqs. (3) and (4) seems to suggest that a unified approach should be possible. Some numeric values are given in Table 1. Plitzko and Mayer [15] measured recently for silicon a mean free path of 880 Å at 120 keV whereas the semi-empirical formula Eq. (4) gives values near 1000 Å [14].

A different approach to the problem is to consider the ratio of the elastic cross section σ_{el} to the inelastic cross section σ_{in}. Egerton [16] derived a simple approximate formula: $\sigma_{in}/\sigma_{en} = \lambda_{el}/\lambda_{in} \approx 17/Z$ where we used $\lambda = 1/N\sigma$ with N the number of atoms per unit volume . Thus, for C the inelastic cross section is larger than the elastic cross section, for Si both are of the same order and for Au the elastic cross section is considerable larger than the inelastic one. Inspection of the ratios of $\lambda_{el}/\lambda_{in}$ in Table 1 show that the values for Au are in reasonable agreement with this formula but for Si and C the obtained value $\lambda_{el}/\lambda_{in}$ is smaller than $17/Z$. In summary there is some uncertainty in the inelastic cross sections in our energy range. In going from light to heavy elements the elastic mean free paths decrease dramatically, whereas the inelastic mean free paths decreases much more modestly.

3. Coincidence count rate for extremely thin samples

Our spectrometer, outlined in Fig. 2, has two electron analysers, each equipped with conical slit input lenses [3] and positioned at 44.3°. Incoming electrons have an energy of 50 keV, momentum 62.07 a.u. (we will often work in atomic units $\hbar = m = c = 1$, multiply momentum values by 1.89 to convert a.u. in Å^{-1}), the scattered and ejected electron have an energy near 25 keV (momentum 43.36 a.u.). The analysers use channel plates/resistive anode detector combination at the exit planes and, at a mean pass energy of 400 eV, detects electrons over a 70 eV range with a resolution of 0.6 eV.

It is instructive to investigate how the count rate in each detector (often referred to as the 'singles count rate') changes as a function of energy (keeping the incoming energy constant at 50 keV). This is shown in Fig. 3 for an extremely thin carbon film. The count rate shows an approximately Gaussian distribution (on a background) with a maximum near 25 keV. This is a Compton profile of the target electron momentum

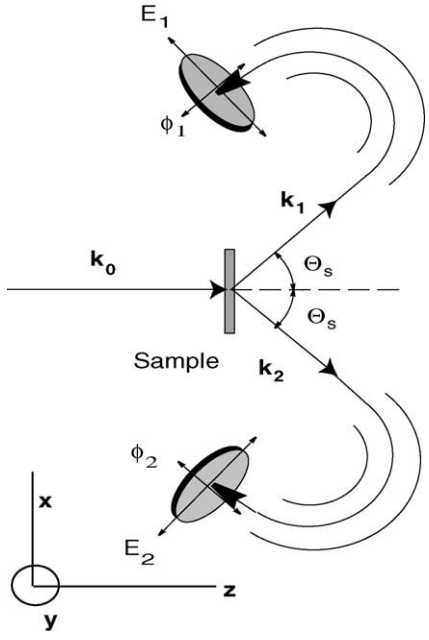

Fig. 2. Schematic representation of the spectrometer.

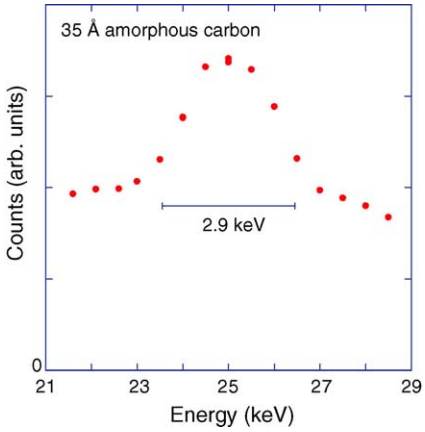

Fig. 3. The count rate in a detector, positioned at 44.3°, as a function of the detected electron energy for 50 keV electrons impinging on a carbon film. The measured count rate reveals a Compton profile of the electron momentum distribution in a carbon film.

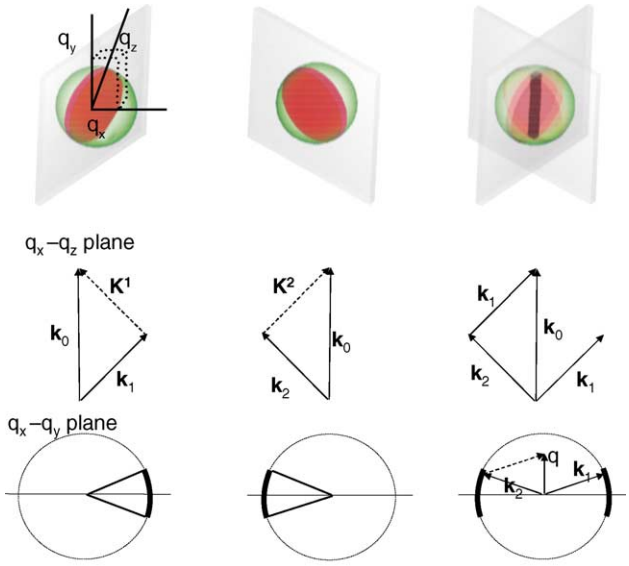

Fig. 4. A representation of an EMS experiment as a combination of two Compton experiment, as explained in the text.

distribution (and this type of measurement has been used to study momentum densities in an electron microscope, see e.g. [17]). The energy loss of the incoming electron (momentum $\mathbf{k}_0$) after scattering from a target electron with momentum $\mathbf{q}$ is given by

$$\Delta E = \frac{|\mathbf{K}|^2}{2m} + \frac{\mathbf{K}\cdot\mathbf{q}}{m}, \tag{5}$$

with m the electron mass and $\mathbf{K} = \mathbf{k}_0 - \mathbf{k}_1$ the momentum transfer, which has a magnitude close to 43.36 a.u. in this experiment. The distribution has a maximum at an energy of 25 keV and here only electrons with $\mathbf{K}\cdot\mathbf{q} = 0$ contribute to the count rate. For a free electron gas with the same electron density as graphite the Fermi sphere radius would be 1.25 a.u. and the base width of the Compton profile is then $2|K|k_f/m = 2.9$ keV, and even this rough model is in reasonable agreement with the experiment. Note that the Compton peak is on a rather constant background. The origin of this constant contribution is not understood. Under (e,2e) conditions about half the singles counts will be due to Compton scattered electrons.

Now, we want to understand the relation between the singles count rate and the (e,2e) count rate (or coincidence count rate), by comparing the phase space that is accessible in a singles (electron Compton) experiment and an (e,2e) experiment. As electrons are indistinguishable particles we do not know if an electron detected in an electron Compton experiment is either the scattered or the ejected electron. However, if we do two Compton experiments simultaneously we can detect coincidences only if the scattered electron is detected in one analyser, and the ejected electron in the other.

The Fermi sphere is displayed in Fig. 4. By detecting electrons in analyser 1 with energies very close to 25 keV we select target electrons with a momentum component along the momentum transfer direction $\mathbf{K}^1$ smaller than 0.1 a.u. (for all electrons within the 70 eV energy window of the analyser) (Fig. 4, left, top panel). These electrons are within the disc intersecting the Fermi sphere in Fig. 4. The width of this disk Δk is determined not only by the range of electrons energies (70 eV) that are detected simultaneously in the detector (70 eV corresponding to 0.06 a.u. in our case) but also to the finite slit width of the analyser (0.5 and 150 mm away from the target) resulting in a (small) range of scattering angles θ. The combined effect is a momentum resolution to about $\Delta k \simeq 0.1$ a.u. Similar considerations hold for singles detected by analyser 2 and its corresponding momentum transfer K^2 (Fig. 4, central, top panel) but the direction of K^2 is nearly perpendicular to K^1.

If we would position the second analyser at an arbitrary angle we would generally see no coincidences, as there is a well-defined relation between the direction of propagation of the scattered and ejected electrons (see Eq. (2)). In the central row of Fig. 4 we show the momenta of the incoming and outgoing electrons of the three experiments, as projected in the $q_z - q_x$ plane. In this plane we have for our choice of scattering angles and energies: $\mathbf{k}_0 = \mathbf{k}_1 + \mathbf{k}_2$. Thus coincidences can only occur for target electrons with $q_x \simeq q_z \simeq 0$ (Fig. 4 right, central panel). In the third row of Fig. 4 we show a projection of the experiment in the $q_z - q_y$ plane. As the detector have slit lenses extending along the y-direction each detector can measure electrons with a range of ϕ values. The momentum transferred to the target in the (e,2e) event $\mathbf{q}$ is directed along the $\mathbf{q_y}$ axis and has magnitude is proportional to $\phi_1 - \phi_2$.

An (e,2e) experiment can be seen as a combination of two Compton experiments. The momentum transfer of the second Compton experiment is perpendicular to that of the first (see Fig. 4 (top, central panel)). Coincidences can only occur for electrons in the overlap of the two Compton disks. It has (for carbon) a volume of $2(\Delta k)^2 k_f = 0.025$ a.u.^{3}, i.e. about 20

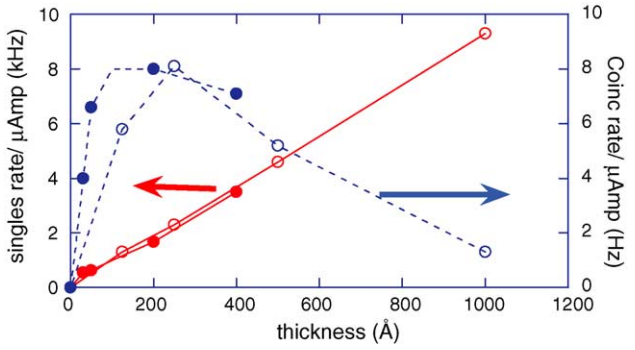

Fig. 5. The singles and coincidence count rate for C (solid circles) and Si (open circles) samples of different thicknesses.

times smaller than the volume that can cause a singles count in each detector.

In Fig. 5, we show the dependence of the count rate for carbon films on thickness. The thicknesses are the nominal values quoted by the supplier, but the linear dependence of the singles count rate on sample thickness confirms these values. The coincidence count rate has a maximum near 200–300 Å. For the thinnest carbon samples the coincidence count rate is 100 times lower than the singles count rate. This corresponds to about 1 coincidence count per 50 Compton-peak related singles events. The very simple model sketched in Fig. 4 predicts 1 coincidence count per 20 singles events. The difference is mainly due to the fact that the disks in Fig. 4 are not measured with 100% efficiency.

4. EMS of samples of larger thickness

In Fig. 5, we see that only for the thinnest samples the coincidence count rate increases linearly with sample thickness. For larger thicknesses the coincidence count rate flattens out and subsequently starts to decrease. However, the singles rate keeps increasing with thickness. The decrease of the coincidence count rate is a consequence of multiple scattering.

If, for example, the scattered electron loses energy by one or more inelastic scattering events it may end up with an energy that is outside the energy window of the analyser, and hence these processes lead a reduction of the count rate. The same is true for elastic multiple scattering. The target electrons have a momentum of typically 1 a.u. which is much smaller than the incoming and outgoing electron momenta. Thus, given a certain direction of $\mathbf{k}_1$ there is only a small range of directions of $\mathbf{k}_2$ allowed. The position of detector 2 relative to detector 1 and the incoming beam direction are chosen in such a way that the coincidence count rate is maximised. Changes in $\mathbf{k}_0$, $\mathbf{k}_1$ or $\mathbf{k}_2$ due to elastic scattering will reduce the degree of correlation between the direction of the emerging electrons, and hence again reduce the coincidence rate.

If either the energy loss due to inelastic scattering or the deflection due to elastic scattering is large then the event will not contribute to the coincidence count rate. Of more importance are those events that, in spite of small deflections and/or energy losses, still lead to a coincidence event, but for which the subsequently inferred binding energy ε and/or momentum $\mathbf{q}$ as obtained using Eqs. (1) and (2) is wrong. This complicates for thicker samples a comparison with theory greatly. In the following section we will simulate the effect of multiple scattering for the case of silicon, and see how the ratio of inelastic and elastic mean free path changes qualitatively the outcome of the simulation.

5. Shape of the observed spectra for silicon crystals with different thicknesses

The optimum thickness for an (e,2e) experiment does not correspond to the thickness with maximum coincidence count rate. Elastic and inelastic multiple scattering do not affect the temporal correlation between the two emerging electrons. For the thicker samples a large fraction of the coincidence events are contaminated by multiple scattering. This fact is dramatically illustrated in Fig. 6 for the case of silicon. Here, we present spectra at zero momentum and momentum densities at the valence band maximum. For the thickest samples the measured intensity increases with increasing binding energy, and these spectra contain very little information about the electronic structure. Only for the thinnest sample does the valence band become the most intense feature. The momentum densities at the valence band maximum are less affected by the thickness, increasing thickness mainly causes a reduction in the absolute intensity. These measurements for the $\langle 1\,1\,1\rangle$ direction show clearly the effect of diffraction: the main peaks at ± 1.0 a.u. is accompanied by minor peaks at 0 a.u. and near 2 a.u., separations corresponding to the smallest reciprocal lattice vector ($|G_{\langle 1\,1\,1\rangle}| = 1.06$ a.u.). The smooth slowly varying intensity in between the main peaks are due to incoherent (thermal diffuse) scattering. For more details on the identification of the diffracted contribution and the result for somewhat thinner films see [10,18].

To test our understanding of these processes we performed Monte Carlo simulations, based on a code that has been described previously [11]. The main difference between this earlier version and the current one is that energy distribution of energy loss events is not taken to be a Gaussian distribution centered around the mean plasmon loss energy, but an energy distribution of which the shape was determined in a separate energy loss experiment of the thinnest film available. These results are shown as well in Fig. 6. Qualitatively the same tendencies are observed in the experiment and in the simulations. The effects of diffraction are not incorporated in the Monte Carlo simulations, which assume that all elastic collisions of different atoms are incoherent. The main discrepancy between experiment and simulation is that the effect of thickness seems to be underestimated in the simulations for the energy spectra. A separate simulation was done with the inelastic mean free paths reduced by a factor of 2. This simulation is indicated by a dashed line in Fig. 6

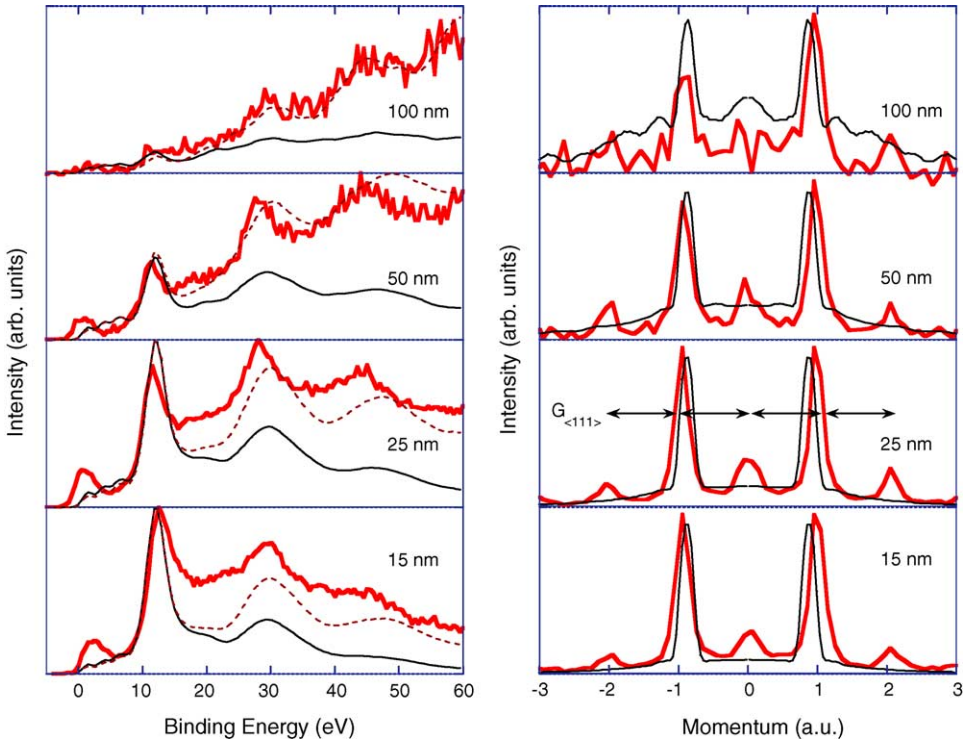

Fig. 6. The dependence of the spectra at zero momentum and the momentum density at the valence band maximum on the thickness of a silicon sample. Simulated spectra (thin line) uses the mean free path as in Table 1. The dashed line in the left panel is for a simulation with the elastic mean free reduced by a factor of 2.

and seems to follow the experiment more closely. A similar agreement for the spectra can be obtained by doubling the assumed sample thickness. However, this would reduce the agreement in the momentum density profiles. Part of this problem could be due to intrinsic satellites. These satellites (due to electron–electron correlation, sometimes referred to as 'intrinsic plasmons') are included in the theory that was used as an input for the Monte Carlo simulations, but the computational scheme used seems to underestimate the intrinsic satellite contribution. A comparison of spectra obtained for silicon, using thinner films, with the results of many-body theory is given elsewhere [18,19].

6. EMS of heavy elements

There are two factors that are unfavourable for EMS of heavy targets, e.g. gold films. The first factor is an expected reduction in the elastic mean free path. Not only is the elastic mean free path about five times smaller in Au compared to Si and C, but also the average scattering angle in a deflection is somewhat larger for Au (see Fig. 1). The second problem is the presence of many electrons in the sample with large momentum values, e.g. the 5d electrons have on average a momentum with a magnitude of several a.u. Thus, their extension in momentum space, as sketched in Fig. 4 is much larger. This causes a reduction of the ratio of coincidences to singles. Moreover many of these core levels (even the shallow ones) will not contribute at all to the coincidence count rate as their binding energy is outside the accessible range, but they still contribute to the Compton profile (i.e. singles count rate).

It was thus surprising that an attempted measurement of the electronic structure of Au was successful, even for single crystalline films. Au layers of 1000 Å thickness were grown on an NaCl crystal. The salt substrate was dissolved, the film floated off, transferred to the sample holder with 0.2 mm diameter holes and subsequently sputter-thinned in situ. The thickness of the film, as estimated from the EELS data, was 70–90 Å, but the sample is not expected to have a uniform thickness, due to the statistical nature of sputtering. For 1 μA incoming beam a singles rate of 5 kHz was obtained and the corresponding coincidence rate was 0.25 Hz. Clearly the ratio between coincidences to singles ratio was as expected much smaller than for thin C and Si samples. Some examples of the momentum distributions and energy spectra obtained are shown in Fig. 7. Surprisingly the experimental data show a large contrast and the background due to multiple scattering seems to be not worse than that for lighter Z elements. Using the Monte Carlo simulation we can estimate which fraction of the (e,2e) events is not accompanied by additional elastic or inelastic multiple scattering events. Only these events contain clear information about the electronic structure of the target. The results of these simulations are presented in Table 2. From this table we conclude that for carbon and silicon we can do (e,2e) measurements up to

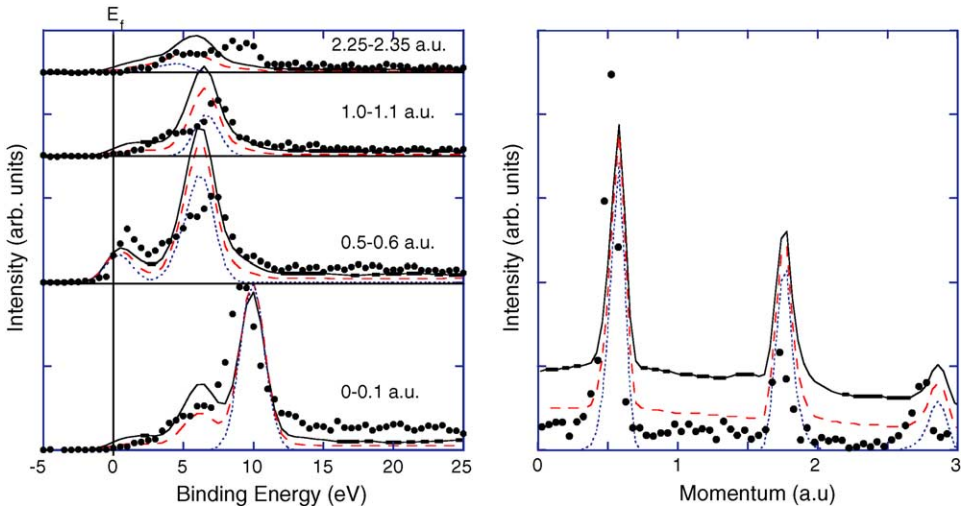

Fig. 7. Spectra at different momentum values as indicated (left panel) as well as the momentum density at E_f (right panel) for Au single crystal films measured along the ⟨1 1 0⟩ direction. The short dashed line corresponds with the (LMTO) theory convoluted with experimental energy and momentum broadening. The long dashed (full) line corresponds to the results of Monte Carlo simulations using the LMTO theory and assuming a thickness of 50 Å(100 Å).

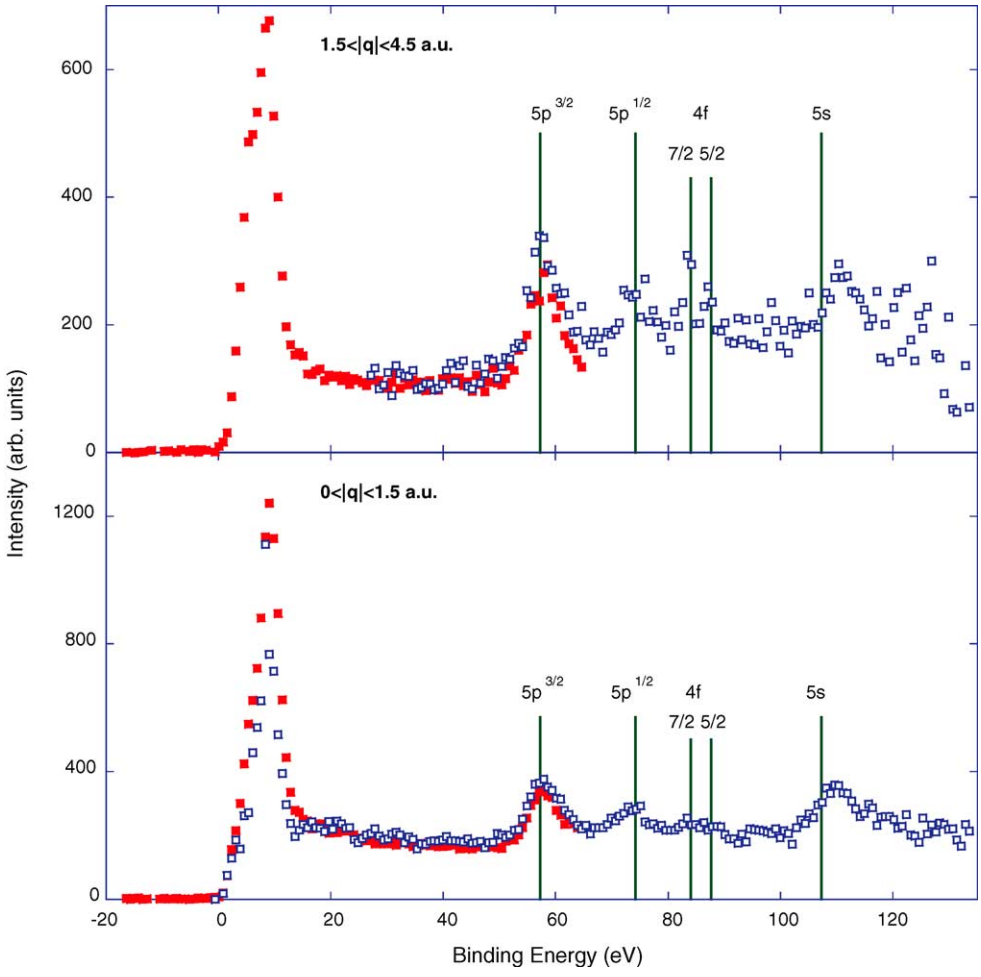

Fig. 8. The measured intensity of a Au film over an extended energy range comprised of two different overlapping scans. The low binding energy scan is presented by filled squares, the scan at higher binding energy by open squares. In the top panel we show the spectra summed over $1.5 < |q| < 4.5$ and in the lower panel we show the intensity summed over low momenta$< |q| < 1.5$ The 4f signal is weak and only visible in the high momentum region. The energy levels shown are taken from [22].

Table 2
The percentage of all (e,2e) events that are it not affected by either elastic or inelastic multiple scattering, as derived from the Monte Carlo simulations

Element	Thickness(Å)	Clean events (%)
Graphite	50	66
Graphite	100	45
Graphite	200	22
Silicon	50	56
Silicon	100	33
Silicon	200	13
Gold	50	9.5
Gold	100	1.6
Gold	200	0.1

thicknesses of 200 Å (at least 10% of the events are clean), but for Au anything above 50 Å appears prohibitively thick. The simulation overestimates the effects of elastic scattering even at 50 Å(see Fig. 7, right panel). A discussion of the measured spectral density for the Au film will be published in a separate paper [20].

Finally, we show in Fig. 8 the spectra for a Au film over a wider energy range. These spectra were obtained from two measurements over a different binding energy window, with a significant overlap. The valence band features are much stronger than the core levels. This is in strong contrast to XPS spectra that are dominated by the core levels. This is a clear illustration of the difference between the ionisation process by photons and by binary collisions of electrons. The very localised core levels have very diffuse momentum-space wave functions. Hence, the density at any given point in momentum space is small, resulting in low-intensity peaks in the EMS spectra. Orbitals with high angular momentum such as the 4f electrons have virtual no density below 1.5 a.u., whereas the 5s electron has maximum density at zero momentum. The momentum distribution of the 5p electrons is in between that of the 4f and 5s. Note that the Au 5s peak is usually not observed in XPS spectra as its intensity is dwarfed by the intense neighbouring 4f lines. The value usually quoted for the 5s binding energy is 107.2 eV [21] was hence derived from the energy separation between different levels as given by Baerden and Burr [22]. Our measurement indicate that the 5s level is at 109.8 ± 0.8 eV binding energy.

7. Conclusion and discussion

We have studied the influence of multiple scattering on EMS measurements. Only for the thinnest films of low Z elements, where multiple scattering probability is small, is the count rate proportional to the sample thickness. Here, we find a coincidence count rate that is about 1% of the singles count rate. We showed that this ratio can be understood in terms of the phase space of electrons that contribute to singles and the coincidence events. For the low Z elements coincidence count rate drops slowly with increasing film thickness, but more importantly the measured intensity distribution is heavily affected by multiple scattering and the spectrum seems to shift to higher and higher binding energies with increasing thickness, due to inelastic energy loss processes. For high Z target the count rate is low, even for thin films, but the spectra appear to be much less affected by multiple scattering than expected.

It is possible to simulate the effect of multiple scattering semi-quantitatively by Monte Carlo. However, generally the effects of elastic multiple scattering are overestimated, whereas the effects of inelastic multiple scattering seems underestimated in these simulations. The first problem could be attributed to a failure of the incoherent approximation. Especially for small scattering angles (when the momentum transfer in the elastic scattering event k_{el} is such that $|1/k_{el}|$ is of the order of the interatomic separation) one should consider the effects of diffraction. Normally Monte Carlo simulations are used to calculate transport properties, which are not severely affected by small angle deflections. However, in the EMS case small deflections cause a significant change in the inferred momentum **q** that is associated with the (e,2e) event. Hence, a more sophisticated approach is required incorporating both the coherent and incoherent elastic scattering processes.

The fact that inelastic scattering appears to be worse in the experiment compared to the simulation could be a consequence of deficiencies in the spectral function used as input for the simulation. For silicon the spectral function used incorporated an estimate of the intrinsic plasmons, whereas this was not the case for Au. In both cases the simulation underestimates the intensity at larger binding energies. Judging from the experiments, intrinsic plasmons should be less important for Au than for C or Si.

Acknowledgments

The authors want to thank Erich Weigold for carefully reading the manuscript. This work was made possible by a grant of the Australian Research Council.

References

[1] E. Weigold, I.E. McCarthy, Electron Momentum Spectroscopy, Kluwer Academic/Plenum, New York, 1999.
[2] I.E. McCarthy, E. Weigold, Rep. Prog. Phys. 54 (1991) 789.
[3] M. Vos, G.P. Cornish, E. Weigold, Rev. Sci. Instrum. 71 (2000) 3831–3840.
[4] M. Vos, A.S. Kheifets, E. Weigold, F. Aryasetiawan, Phys. Rev. B 63 (2001) 033108.
[5] M. Vos, A.S. Kheifets, V.A. Sashin, E. Weigold, M. Usuda, F. Aryasetiawan, Phys. Rev. B 66 (2002) 155414.
[6] E. Weigold, A.S. Kheifets, V.A. Sashin, M. Vos, Acta Cryst. A60 (2004) 104–110.
[7] L.J. Allen, I.E. McCarthy, V.W. Maslen, C.J. Rossouw, Aust. J. Phys. 43 (1990) 453–464.
[8] R. Matthews, Ph.D. Thesis, Flinders University of South Australia, 1993.

[9] Z. Fang, R.S. Matthews, S. Utteridge, M. Vos, S.A. Canney, X. Guo, I.E. McCarthy, E. Weigold, Phys. Rev. B 57 (1998) 12882–12889.
[10] M. Vos, A.S. Kheifets, V.A. Sashin, E. Weigold, J. Phys. Chem. Solids 64 (2003) 2507–2515.
[11] M. Vos, M. Bottema, Phys. Rev. B 54 (1996) 5946–5954.
[12] F. Salvat, R. Mayol, Comp. Phys. Commun. 74 (1993) 358.
[13] S. Tanuma, C. Powell, D. Penn, Surf. Interface Anal. 17 (1991) 911–926.
[14] T. Malis, S. Cheng, R. Egerton, J. Electron Micros. Tech. 8 (1988) 193.
[15] J.M. Plitzko, J. Mayer, Ultramicroscopy 78 (1999) 207–219.
[16] R.F. Egerton, Electron Energy-loss Spectroscopy in the Electron Microscope, Plenum Press, New York, 1986.
[17] B.G. Williams, T.G. Sparrow, R.F. Egerton, Proc. R. Soc. A 393 (1984) 409–422.
[18] C. Bowles, A. Kheifets, V. Sashin, M. Vos, E. Weigold, J. Electron. Spec. Rel. Phenom. 141 (2004) 95–104.
[19] A.S. Kheifets, V.A. Sashin, M. Vos, E. Weigold, F. Aryasetiawan, Phys. Rev. B 68 (2003) 233205.
[20] M. Vos, C. Bowles, A.S. Kheifets, M.R. Went, unpublished.
[21] M. Cardona, L. Ley (Eds.), Photoemission in Solids I: General Principles, Springer-Verlag, Berlin, 1978.
[22] J.A. Bearden, A.F. Burr, Rev. Mod. Phys. 39 (1967) 125.